Available online at www.sciencedirect.com
ScienceDirect
Journal of Sound and Vibration 315 (2008) 721–731
JOURNAL OF SOUND AND VIBRATION
www.elsevier.com/locate/jsvi

Vibration isolation using extreme geometric nonlinearity

L.N. Virgin[a,*], S.T. Santillan[b], R.H. Plaut[c]

[a]Department of Civil and Environmental Engineering, Duke University, Durham, NC 27708-0287, USA
[b]Department of Mechanical Engineering, United States Naval Academy, Annapolis, MD 21402, USA
[c]Department of Civil and Environmental Engineering, Virginia Polytechnic Institute and State University, Blacksburg, VA 24061-0105, USA

Accepted 13 December 2007
The peer review of this article was organised by the Guest Editor
Available online 19 February 2008

Abstract

A highly deformed, slender beam (or strip), attached to a vertically oscillating base, is used in a vibration isolation application to reduce the motion of a supported mass. The isolator is a thin strip that is bent so that the two ends are clamped together, forming a loop. The clamped ends are attached to an excitation source and the supported system is attached at the loop midpoint directly above the base. The strip is modeled as an elastica, and the resulting nonlinear boundary value problem is solved numerically using a shooting method. First the equilibrium shapes of the loop with varying static loads and lengths are studied. The analysis reveals a large degree of stiffness tunability; the stiffness is dependent on the geometric configuration, which itself is determined by the supported mass, loop length, and loop self-weight. Free vibration frequencies and mode shapes are also found. Finally, the case of forced vibration is studied, and the displacement transmissibility over a large range of forcing frequencies is determined for varying parameter values. Experiments using polycarbonate strips are conducted to verify equilibrium and dynamic behavior.

1. Introduction

Highly deformed elastica structures can be used to support a static load and mitigate the transmissibility of a dynamic vertical excitation [1]. If the base is moving, the purpose of the elastica structure is to minimize the vibrations of the supported system. If the supported system is vibrating, the purpose is to reduce the dynamic force transmitted into the base.

In this paper, the analysis of the static response and subsequent dynamic behavior is based on the elastica model and solutions of the resulting nonlinear boundary value problem. Convenient use can be made of numerical solution techniques, e.g., the shooting method or finite differences, and software packages such as Matlab [2,3]. For example, a thin beam clamped at both ends and then deformed by moving the ends toward each other is a convenient means of varying spring stiffness, if this structure is then used to support a load. In general, the resistance to the application of a vertical excitation depends on the geometric configuration. The

*Corresponding author. Tel.: +1 919 660 5342; fax: +1 919 660 5219.
E-mail address: l.virgin@duke.edu (L.N. Virgin).

0022-460X/$ - see front matter © 2008 Elsevier Ltd. All rights reserved.
doi:10.1016/j.jsv.2007.12.025

extent of deformation, or some other geometric aspect of the system, can then be used to tailor stiffness behavior to achieve desirable isolator characteristics. This concept is related to a discrete analog, sometimes referred to as a zero- or negative-stiffness system [4].

Experimental results offer some practical verification of this approach. The experiments use polycarbonate strips supporting a mass and undergoing base excitation. It is shown that this inherently nonlinear approach offers compelling advantages over a conventional linear-system approach.

2. Background

It has long been recognized that there are certain advantages to having a degree of control over the stiffness elements in a vibration isolation system. For example, if the dominant frequency of the forcing changes with time, it may be desirable to adjust the first natural frequency of the isolator.

Fig. 1 shows schematically the way in which a nonlinear stiffness might be introduced. The stiffness characteristics may be of the hardening (part b) or initially softening (part c) type. However, the conventional approach to designing a nonlinear spring typically involves helical springs [5] with varying pitch or diameter, and these systems provide a limited range of flexibility, are not necessarily easy to manufacture, and (as with other nonlinear systems) must be carefully examined in order to avoid undesirable consequences.

There have been other attempts to take advantage of nonlinearity in a vibration isolation context. A zero-spring-rate suspension system [6] was developed in which a clever arrangement of (linear) springs acted together such that, under pre-load, they behaved in a nonlinear geometric sense. The system is essentially the same as a negative-stiffness mechanism described by Platus [4] and developed commercially. Other approaches have been studied by Zhang et al. [7] and Carrella et al. [8].

Consider a highly deformed elastica structure that will support a static load and act as a vibration isolator. Fig. 2 illustrates the type of system that will receive particular attention in this paper. The self-weight of the loop is included in the analysis. Symmetric equilibria and motions are considered.

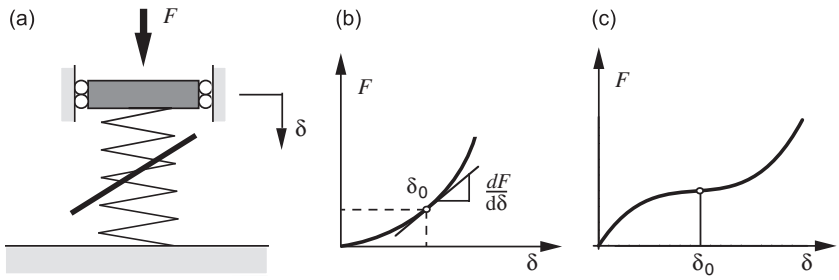

Fig. 1. Example of a nonlinear spring with variable characteristics: (a) schematic, (b) linearized stiffness, and (c) a slope near zero.

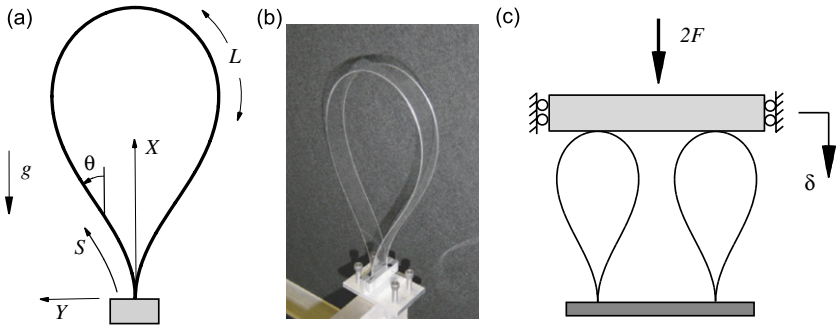

Fig. 2. A thin elastic strip with the ends pushed together: (a) geometry, (b) photographic image, and (c) alternative symmetric configuration.

3. Analytical formulation

The highly nonlinear elastica description is amenable to numerical solutions, including dynamic analyses for small-amplitude motion about highly deflected equilibria [2]. The equations governing the elastic behavior of this system are cast in terms of arc-length coordinates (S,θ), with appropriate boundary conditions. They can be solved numerically using the shooting method, including the effect of self-weight gravity loading if desired. Suppose the initially flat beam has a length L, flexural rigidity EI, and weight (per unit length) W. As shown in Fig. 2(a), points on the loop have coordinates $X(S,T)$ and $Y(S,T)$, where T is time. The X-axis is parallel to the loop at the clamped end. The internal forces in the strip are denoted $P(S,T)$ and $Q(S,T)$ parallel to the X and Y axes, respectively, and the bending moment is $M(S,T)$. A downward point load, F, is applied at the apex of the loop via the mass of the supported system. A viscous damping coefficient, C, is used to model system damping.

In the analysis of this type of system, it is convenient to nondimensionalize the length variables in the problem using the parameter $a=(EI/W)^{1/3}$, and to write the nondimensional length as l, where $l=L/a$ [2]. This nondimensionalization is valid for any nonzero weight per unit length, $W>0$. The remaining nondimensional parameters are defined by

$$\begin{aligned} &s=S/a, \quad x=X/a, \quad y=Y/a, \quad t=T\sqrt{g/a},\\ &\Omega=\omega\sqrt{a/g}, \quad c=C\sqrt{a^7 g}/EI, \quad f=Fa^2/EI,\\ &q=Qa^2/EI, \quad m=Ma/EI, \quad p=Pa^2/EI, \end{aligned} \tag{1}$$

where ω is a dimensional vibration frequency. The governing elastica equations using the defined nondimensional parameters are:

$$\begin{aligned} &\partial x/\partial s=\cos\theta, \quad \partial y/\partial s=\sin\theta,\\ &\partial\theta/\partial s=m, \quad \partial m/\partial s=q\cos\theta-p\sin\theta,\\ &\partial p/\partial s=-1-\partial^2 x/\partial t^2-c\partial x/\partial t, \quad \partial q/\partial s=-\partial^2 y/\partial t^2-c\partial y/\partial t. \end{aligned} \tag{2}$$

Each of the variables is written in the form [9]

$$\begin{aligned} &x(s,t)=x_e(s)+x_d(s)e^{i\Omega t}, \quad y(s,t)=y_e(s)+y_d(s)e^{i\Omega t},\\ &\theta(s,t)=\theta_e(s)+\theta_d(s)e^{i\Omega t}, \quad m(s,t)=m_e(s)+m_d(s)e^{i\Omega t},\\ &p(s,t)=p_e(s)+p_d(s)e^{i\Omega t}, \quad q(s,t)=q_e(s)+q_d(s)e^{i\Omega t}, \end{aligned} \tag{3}$$

where the subscripts e and d denote equilibrium and dynamic components, respectively. The resulting equilibrium equations are:

$$x_e'=\cos\theta_e, \quad y_e'=\sin\theta_e, \quad \theta_e'=m_e, \quad m_e'=q_e\cos\theta_e-p_e\sin\theta_e, \tag{4}$$

where a prime denotes differentiation with respect to s. The forces may be written as

$$p_e(s)=p_o-s, \quad q_e(s)=q_o, \tag{5}$$

where p_o and q_o are constants.

For specified parameter values, the equilibrium shape is found, and Eqs. (3) are substituted into Eqs. (2), using equilibrium equations (4) and (5). The resulting linearized vibration equations are:

$$\begin{aligned} &x_d'=-\theta_d\sin\theta_e, \quad y_d'=\theta_d\cos\theta_e,\\ &\theta_d'=m_d, \quad m_d'=(q_d-p_e\theta_d)\cos\theta_e-(p_d+q_e\theta_d)\sin\theta_e,\\ &p_d'=\Omega^2 x_d-i\Omega c x_d, \quad q_d'=\Omega^2 y_d-i\Omega c y_d. \end{aligned} \tag{6}$$

Eqs. (4) and (6) are solved numerically, and the results are compared with experimental results.

4. Experiments

Thin polycarbonate strips were used in the experiments. The specific weight was $11.2\,\mathrm{kN/m^3}$ and Young's modulus was 2.4 GPa. The strips were 25.4 mm wide and 0.508 mm thick, giving a nondimensional parameter value $a = 0.167$. The ends of each strip were clamped, and the base was attached to the shaker (*MB Dynamics PM50A Vibration Exciter*) that moved vertically, as shown in Fig. 3. At the midpoint of the strip, a vertically sliding mass was attached, where the mass could be varied to simulate specific point load values. For equilibrium measurements, the vertical deflection of the strip's midpoint was recorded for varying mass values. To simulate negative pre-load values, $f < 0$, the experimental system was arranged so that a mass created an upward force at the midpoint. For dynamic measurements, a point-to-point laser vibrometer (*Ometron VH300 +*) was used to measure the velocities of both the loop midpoint and the base (or shaker). The resulting data were used to generate frequency spectra. The shaker frequency was configured for a slow sine wave sweep with frequencies from 1 to 250 Hz.

5. Results

5.1. Equilibrium

Given the assumed structural symmetry of the loop (with a constraint against horizontal motion at the midpoint, $s = l/2$), it is sufficient to numerically analyze only half of the strip, so that $0 \leqslant s \leqslant l/2$, where the point load at $s = l/2$ is $f/2$.

For the equilibrium solution, the nondimensional length, l, and supported system mass parameter, f, are specified, and numerical integration is performed using a shooting method along $0 \leqslant s \leqslant l/2$ to satisfy $x_e(0) = y_e(0) = \theta_e(0) = y_e(l/2) = 0$, $\theta_e(l/2) = -\pi/2$, and $p_e(l/2) = f/2$. The resulting vertical mass deflection (or vertical deflection of the loop at $s = l/2$) is called δ, where

$$\delta = x_e(l/2)|_{f=0} - x_e(l/2). \tag{7}$$

Solving the boundary value problem with $f = 0$ (for the case $l = 2$) results in the equilibrium configuration given by the uppermost curve in Fig. 4(a). If a downward point load f is applied to the apex of the loop, the equilibrium configuration changes. The other curves in Fig. 4(a) show static shapes for load increments of $f = 10, 20, 30, \ldots, 90, 98.6$. The final curve corresponding to $f = 98.6$ gives the static configuration just before self-contact. The second curve from the top in Fig. 4(b) corresponds to Fig. 4(a) ($l = 2$) in a plot of f vs. δ. The other curves correspond to loops of varying lengths. Each curve is continued until self-contact occurs.

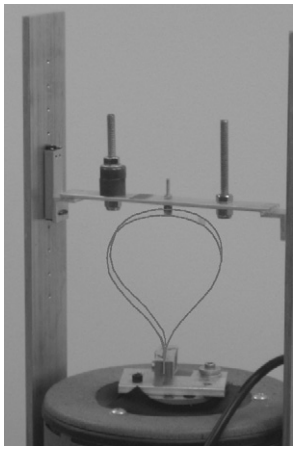

Fig. 3. The experimental vibration isolation system.

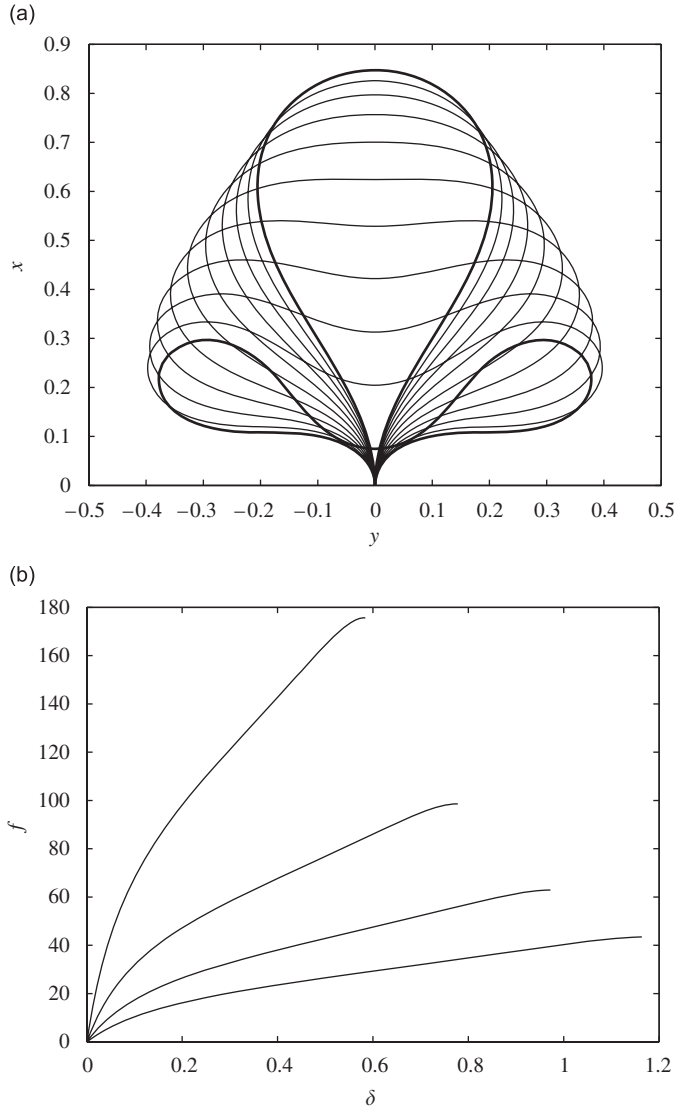

Fig. 4. Numerical equilibrium results: (a) static configurations for $l = 2$ and $f = 0$ (uppermost curve), $10, 20, \ldots, 90, 98.6$, (b) force–deflection curves for lengths $l = 1.5$ (uppermost curve), 2, 2.5, 3.

Load–deflection results for $l = 1.7416$ are shown in Fig. 5, where the data points represent experimental data. Note that upward loads (i.e., $f < 0$) are included. It can be seen that for a compressive load applied at the peak of the loop the local stiffness (slope of the load–deflection curve) can be made relatively small. The loop spring constant is then defined as the local slope in the force–deflection relation.

Fig. 6 shows the computed initial spring constant, where now the vertical stiffness $k = \mathrm{d}f/\mathrm{d}\delta$ is determined by the length of the loop. Results are plotted for four specific pre-load values f. Not surprisingly, the longer the loop, the less stiff it is (in the vertical direction) for a given point force. (The upright configuration of the loop may lose stability for long lengths [2], but in this study the arc length is kept below the critical value.) Hence, the pre-load (which might for example correspond to the dead-weight of the system to be isolated) can be used to tailor the stiffness to a value suitable for isolation. Alternatively, the stiffness may be tailored by changing the length of the loop. Thus the central theme of this approach is that the stiffness of the elastic springs may be adjusted either by changing the pre-load or the overall length of the structure to achieve effective vibration isolation.

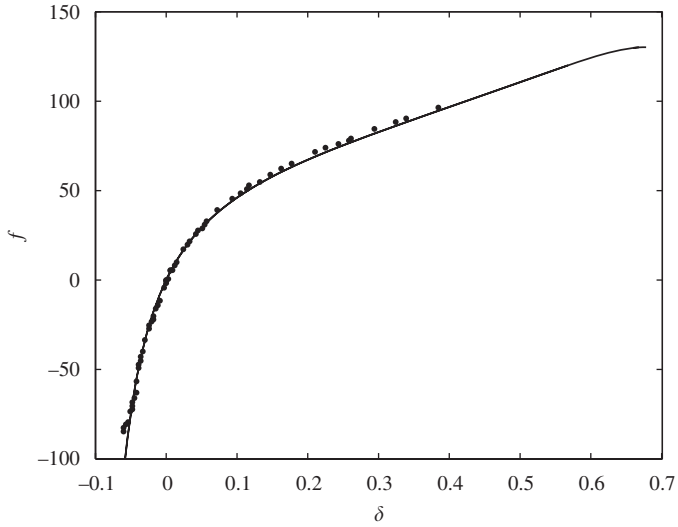

Fig. 5. Force–deflection curve for $l = 1.7416$. Solid curve: numerical results; data points: experimental results.

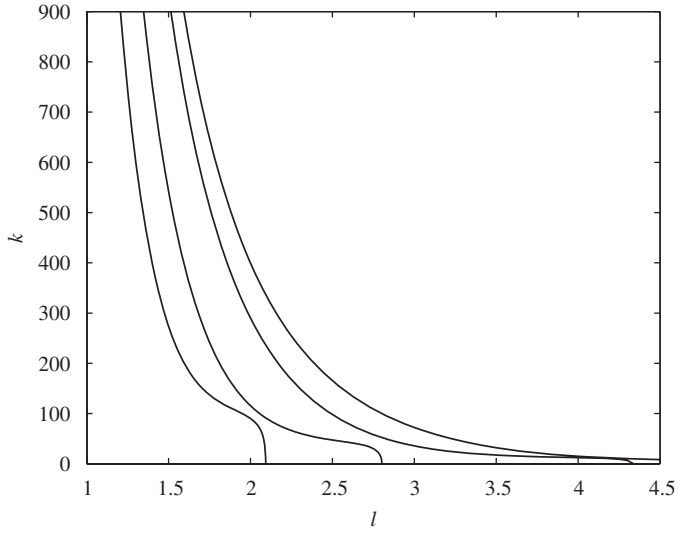

Fig. 6. Vertical stiffness ($k = \mathrm{d}f/\mathrm{d}\delta$) as a function of length, l, for (from left to right) $f = 90$, 50, 20, 10.

5.2. Free vibration

Free vibration frequencies and mode shapes for the system are found using the equilibrium solution (for given values of l and f and $c = 0$), Eqs. (6), and the shooting method to satisfy $x_d(0) = y_d(0) = \theta_d(0) = y_d(l/2) = \theta_d(l/2) = 0$ and $p_d(l/2) = -(f/2)\Omega^2 x_d(l/2)$. The first frequency is plotted in Fig. 7 for the four nondimensional lengths $l = 3$, 2.5, 2, and 1.5. For each length, the fundamental frequency is found up to self-contact, which, for $l = 3$ and 2.5, occurs before the system becomes unstable. When this occurs, the frequency drops to zero, and the structure is unable to statically support the mass.

The first three natural frequencies as a function of f are shown in Fig. 8 for $l = 2$ (up to self-contact). With no pre-load ($f = 0$), these natural frequencies for this case are $\Omega_1 = 21.13$, $\Omega_2 = 59.59$, and $\Omega_3 = 120.56$. The first two frequencies decrease, whereas the third frequency decreases initially, reaches a minimum at $f = 66.7$, and then increases for larger mass values. The corresponding loop isolator mode shapes are shown in Fig. 9

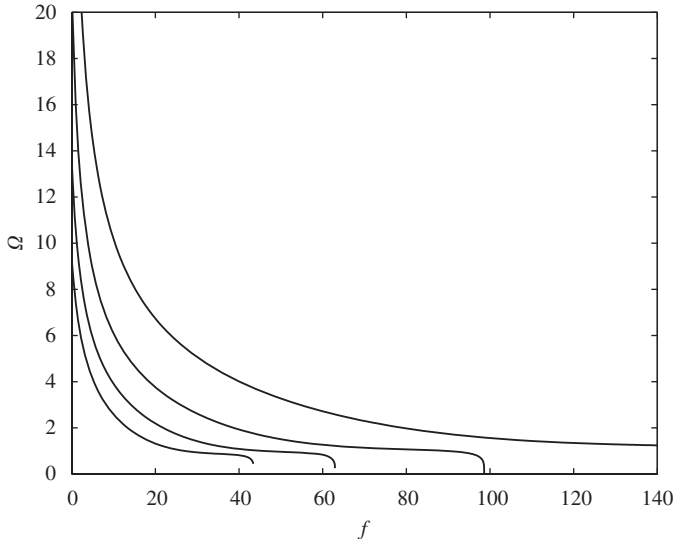

Fig. 7. First frequency as a function of f for (from left to right) $l = 3$, 2.5, 2, 1.5.

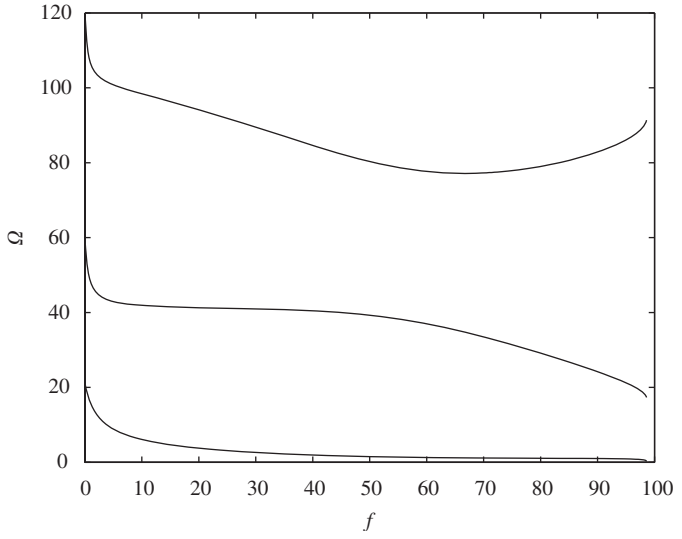

Fig. 8. First three natural frequencies as a function of f with $l = 2$.

for $l = 2$ and $f = 10$ (giving $\delta = 0.021$), where the dashed curve gives the equilibrium configuration. The resulting nondimensional frequencies for this case are $\Omega_1 = 6.09$, $\Omega_2 = 41.89$, and $\Omega_3 = 98.40$.

5.3. Vibration isolation

Forced vibration is considered by assuming a base excitation, $u(t)$, that is sinusoidal, i.e.,

$$u(t) = u_o \sin \Omega t. \tag{8}$$

The nondimensional forcing amplitude, u_o, is defined as $u_o = U_o/a$, where U_o is the dimensional excitation amplitude. Numerical results may again be found by numerically integrating Eqs. (6). Here, the forcing amplitude, u_o, and frequency, Ω, are specified, and the shooting method is used to satisfy $x_d(0) = u_o$, $y_d(0) = \theta_d(0) = y_d(l/2) = \theta_d(l/2) = 0$, and $p_d(l/2) = -(f/2)\Omega^2 x_d(l/2)$. The resulting displacement transmis-

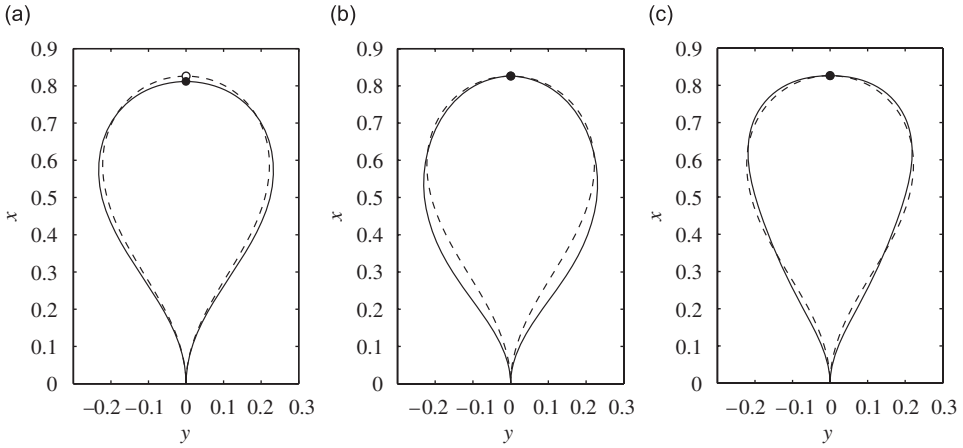

Fig. 9. Mode shapes for $l = 2$ and $f = 10$ ($\delta = 0.021$). Dashed curve and open circle: equilibrium; solid curves and closed circles: mode shape. The first three natural frequencies are: (a) $\Omega_1 = 6.09$, (b) $\Omega_2 = 41.89$, and (c) $\Omega_3 = 98.40$.

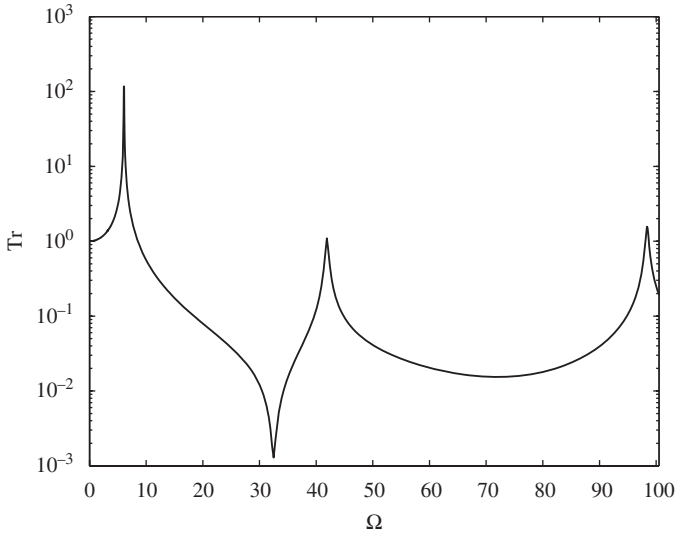

Fig. 10. Numerical transmissibility results for $l = 2$, $f = 10$, and $c = 0.5$.

sibility is then defined as

$$\mathrm{Tr} = \frac{|x_d(l/2)|}{u_o}. \tag{9}$$

Numerical transmissibility results for $l = 2$, $f = 10$, and $c = 0.5$ are shown in Fig. 10. The dynamic vibration shapes corresponding to the first three transmissibility peaks are similar to the first three mode shapes.

Experimental transmissibility results are shown in Figs. 11 and 12, where the smooth curve represents numerical results found using the given parameter values and $c = 1$. Fig. 11 presents results for a nondimensional length $l = 1.987$, where $f = 29.29$ in (a) and $f = 44.60$ in (b). The natural frequencies for this case are found numerically using the free vibration equations, giving 3.33, 50.74, and 111.45 Hz for $f = 29.29$, and 2.13, 49.62, and 102.45 Hz for $f = 44.60$. The experimental transmissibility peaks occur at 3.68, 52.56, and 120.47 Hz for $f = 29.29$, and 2.56, 51.63, and 112 Hz for $f = 44.60$.

In Fig. 12, results for $l = 1.479$ are plotted, where $f = 29.29$ in (a) and $f = 44.60$ in (b). The numerically computed natural frequencies are 6.49, 91.93, and 214.10 Hz for $f = 29.29$, and 4.60, 91.50, and 206.19 Hz for

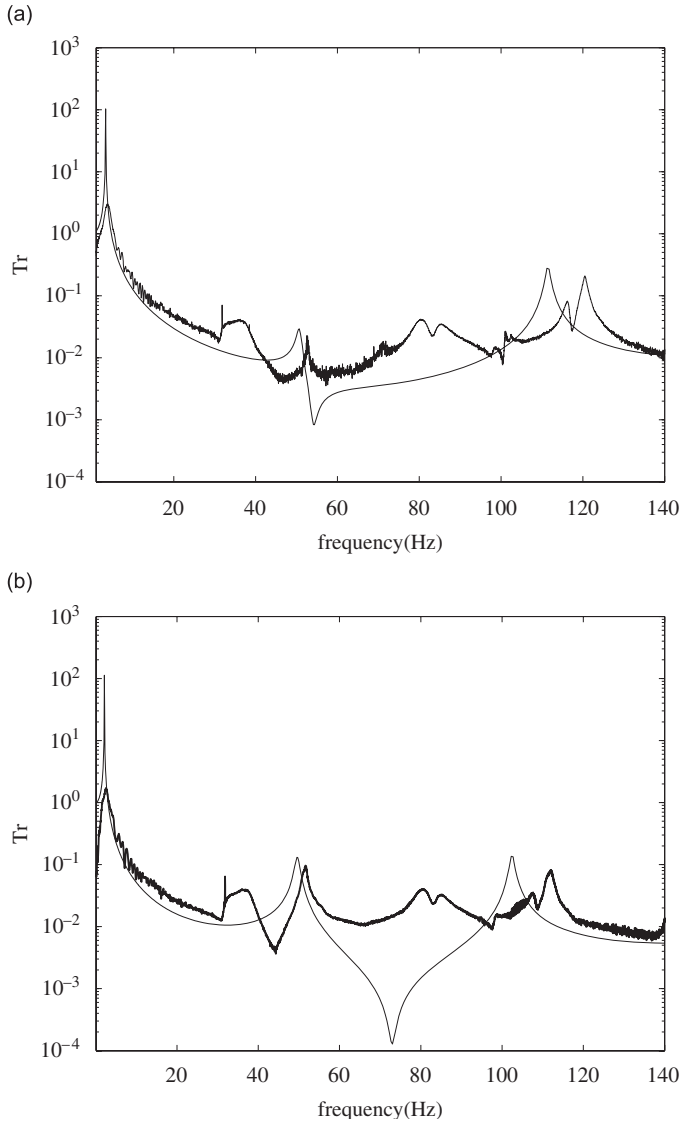

Fig. 11. Experimental and numerical transmissibility results, $l = 1.987$: (a) $f = 29.29$, (b) $f = 44.60$.

$f = 44.60$. The experimental transmissibility peaks occur at 6.81, 94.25, and 222.06 Hz for $f = 29.29$, and 4.94, 94.19, and 215.88 Hz for $f = 44.60$. Although experimental peaks occur near the numerically computed natural frequencies, anti-resonances do not appear in the experimental measurements. Because anti-resonances correspond to very small amplitudes of motion, experimental measurements at these frequencies are more vulnerable to noise, making such local minima difficult to detect [10].

In both the numerical and experimental results, there is a considerable attenuation of the transmissibility for forcing frequencies above the first resonance, and this resonant frequency can be tuned by either altering the loop length or static mass of the system.

In the experimental results for each case, there are some additional transmissibility peaks that do not appear in the numerical results. These peaks may correspond to vibration shapes with rotation at the midpoint (where, in the analysis, it is assumed that $\theta(l/2, t) = -\pi/2$). The attachment point of the mass also has a finite width in the experiments, whereas the analysis assumes that this force is applied as a point load. Finally, there may be some asymmetry in the experimental system due to an error in the attachment point location of the mass.

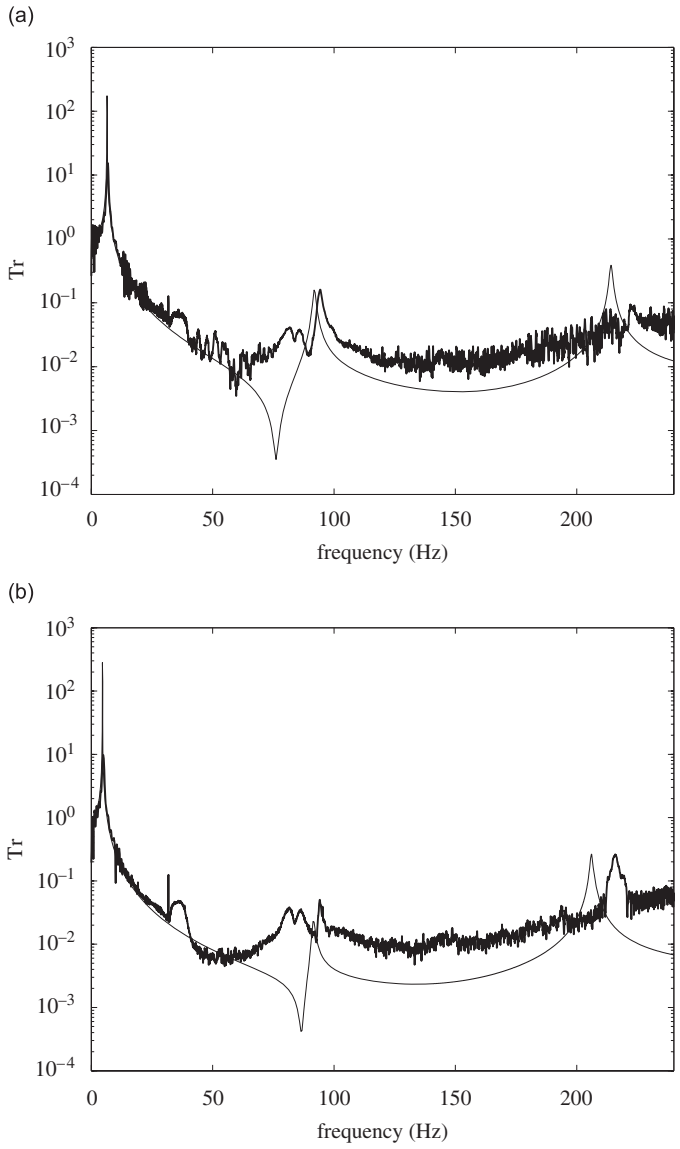

Fig. 12. Experimental and numerical transmissibility results, $l = 1.479$: (a) $f = 29.29$, (b) $f = 44.60$.

While in this case the mass motion is constrained to be purely vertical, the pinched loop isolator system is one that may also be studied as a horizontal motion isolator or even a system that isolates motion in both directions simultaneously. This system characteristic makes the pinched loop isolator particularly advantageous over a helical spring system, where the motion must be limited to be exclusively in one direction.

6. Conclusions

The concept of using highly deformed continuous elastic structures as spring elements in a vibration isolation context was studied. The pinched loop was considered, and governing equations were derived using an elastica analysis. With the assumption of symmetry, the equations were solved numerically using a shooting method to satisfy the boundary conditions. Equilibrium configurations and in-plane free and forced vibrations were examined. The mass (applied at the midpoint of the loop) and the loop length were varied.

If the mass is fixed and the length is increased, the loop becomes less stiff vertically. Increasing the mass and fixing the length also produces a decrease in the stiffness. By changing the loop length and/or the system mass, the stiffness may easily be adjusted. The first natural frequency of the system, then, changes significantly depending on the system parameters. This frequency was found numerically for varying lengths and masses up to self-contact. Numerical displacement transmissibility results indicate that the system is an effective isolator for forcing frequencies beyond the first natural frequency. Experimental data agreed well with the analytical results.

Although the governing equations are somewhat more difficult to solve than the equations governing linear springs, the solutions are essentially exact. By appropriate adjustment of system parameters, the pinched loop provides a viable means of isolating a mass from a vertically oscillating base.

References

[1] L.N. Virgin, R.B. Davis, Vibration isolation using buckled struts, *Journal of Sound and Vibration* 260 (2003) 965–973.
[2] S. Santillan, L.N. Virgin, R.H. Plaut, Equilibria and vibration of a heavy pinched loop, *Journal of Sound and Vibration* 288 (2005) 81–90.
[3] S.T. Santillan, L.N. Virgin, R.H. Plaut, Post-buckling and vibration of heavy beam on horizontal or inclined rigid foundation, *Journal of Applied Mechanics* 73 (2006) 664–671.
[4] D.L. Platus, Negative-stiffness-mechanism vibration isolation systems, *Proceedings of SPIE, Vibration Control in Microelectronics, Optics, and Metrology*, Vol. 1619, 1992, pp. 44–54.
[5] E.I. Rivin, Vibration isolation of precision objects, *Sound and Vibration* 40 (2006) 12–20.
[6] S.E. Woodard, J.M. Housner, Nonlinear behavior of a passive zero-spring-rate suspension system, *Journal of Guidance, Control, and Dynamics* 14 (1991) 84–89.
[7] J.Z. Zhang, D. Li, M.J. Chen, S. Dong, An ultra-low frequency parallel connection nonlinear isolator for precision instruments, *Key Engineering Materials* 257–258 (2004) 231–236.
[8] A. Carrella, T.P. Waters, M.J. Brennan, Optimization of a passive vibration isolator with quasi-zero-stiffness characteristic, University of Southampton, Institute of Sound and Vibration Research Memorandum ISAV 960, 2006.
[9] R.H. Plaut, H.M. Favor, A.E. Jeffers, L.N. Virgin, Vibration isolation using buckled or pre-bent columns. Part 1: two-dimensional motions of horizontal rigid bar, *Journal of Sound and Vibration* 310 (2008) 409–420.
[10] D.J. Ewins, *Modal Testing: Theory and Practice*, Wiley, London, 1984.